An optical synchronous up counter based on electro-optic effect of lithium niobate based Mach–Zehnder interferometers

Citation: Kumar, Santosh et al. “An Optical Synchronous up Counter Based on Electro-Optic Effect of Lithium Niobate Based Mach–Zehnder Interferometers.” Optical and Quantum Electronics 47.11 (2015): 3613–3626.

Published Version: http://dx.doi.org/10.1007/s11082-015-0234-y

Publisher: Springer US

Permanent Link: http://hdl.handle.net/1721.1/105887

Version: Author's final manuscript: final author’s manuscript post peer review, without publisher’s formatting or copy editing

Opt Quant Electron (2015) 47:3613–3626
DOI 10.1007/s11082-015-0234-y

An optical synchronous up counter based on electro-optic effect of lithium niobate based Mach–Zehnder interferometers

Santosh Kumar[1] · Gurdeep Singh[1] · Ashish Bisht[1] · Angela Amphawan[2,3]

Received: 17 June 2015 / Accepted: 14 July 2015 / Published online: 26 July 2015

Abstract Sequential circuits have the ability to store, retain and then retrieve information when needed at a later time. They act as storage elements and have memory. However, due to ever increasing demand of data rate, already existing electronic signal processing devices have become obsolete due to their large latency. To overcome the existing bottleneck, a 4-bit synchronous up counter using electro-optic effect of Mach–Zehnder interferometer has been proposed. The study is carried out by simulating the proposed device with beam propagation method.

Keywords Sequential circuits · Optical switching device · Lithium niobate · Mach–Zehnder interferometer (MZI) · Beam propagation method (BPM)

1 Introduction

To deal with the high requirement for data traffic, optics has till date settled its effectiveness in various arithmetic and logic operations (Li et al. 1999; Sokoloff et al. 1993; Wang et al. 2002; Shen and Wu 2008; Vikram and Caulfield 2005) due to its key features of large bandwidth (Caulfield 1990), EMI immunity, massive parallel interconnectivity (Caulfield 1990), low power consumption (Caulfield and Shamir 1989; Caulfield and Collins 1989) and high speed (Caulfield and Shamir 1990; Caulfield 1990; Goodman et al. 1984). These advantages can help us to accomplish our dream goal of constructing an

✉ Santosh Kumar
santoshrus@yahoo.com

[1] Photonics Lab, Department of Electronics and Communication Engineering, DIT University, Dehradun 248009, India

[2] Fulbright Research Fellow, Massachusetts Institute of Technology, Cambridge, MA 02139, USA

[3] InterNetWorks Research Laboratory, School of Computing, Universiti Utara Malaysia, 06010 Sintok, Kedah, Malaysia

ultra-fast computer that can surpass the fastest possible computer. In this regard, many researchers have shown their keen interest in implementing an optical binary counter. First of all, a 100 MHz optical counter was constructed (Feuerstein et al. 1991) that used directional coupler switches and operated with both 4-bit and 6-bit counts by using two different counter designs. Optical binary counters using SOA-MZIs in different configurations have been demonstrated (Wang et al. 2009; Kaur and Kaler 2014; Poustie et al. 2000). But, owing to the limitation of gain saturation in SOA-MZI, the performance of the device gets hindered. To overcome this limitation, in this paper, authors have demonstrated the design for an optical counter based on electro-optic (EO) effect of $LiNbO_3$ based Mach–Zehnder interferometer (MZI). $LiNbO_3$ based MZI is characterized by the attractive features of compact size, thermal stability (Wooten et al. 2000), re-configurability (Jin et al. 2014), integration potential (Wooten et al. 2000), low latency and low power consumption (Singh et al. 2012; Kumar et al. 2015b). Due to which many researchers have shown their keen interest and designed various combinational and sequential circuits using MZIs (Kumar et al. 2013, 2014a, b, 2015a, b; Raghuwanshi et al. 2013, 2014). Design of 2-bit asynchronous down counter using EO effect of MZI was proposed (Raghuwanshi et al. 2014), where authors had obtained $\bar{Q}_n$ from Q_n itself (by placing a photo-detector after Q_n and giving that output electrical signal to second electrode of another MZI, which acts as an inverter and second output of that MZI gives us $\bar{Q}_n$). Doing so, there is a limitation in implementing any sequential logic circuit that makes use of $\bar{Q}_n$, because, as we convert Q_n into an electrical signal and then apply that electrical signal to another electrode, there is a

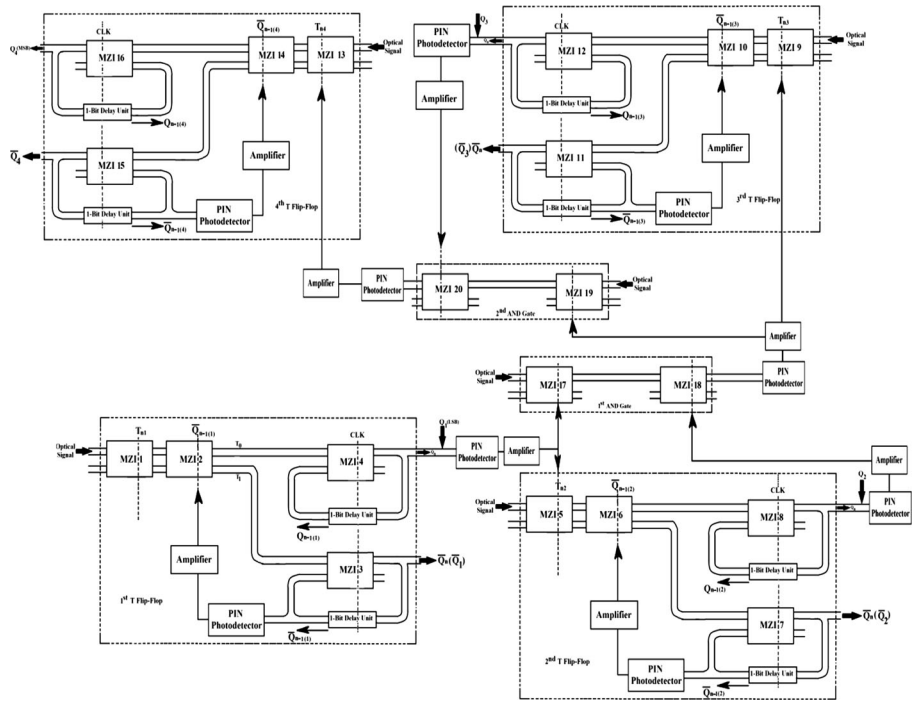

Fig. 1 Schematic diagram of a 4-bit synchronous up counter

certain amount of delay to obtain $\bar{Q}_n$ due to which, a limitation on switching speed of input data (T_n) is imposed.

This paper outlines the design process of a synchronous up counter based on the EO effect of integrated MZIs. The proposed device is simulated by beam propagation method (BPM). The basic working principle of the proposed device is presented in Sect. 2. The mathematical expressions and results obtained through BPM and their discussions are well presented in Sects. 3 and 4 respectively. Finally, Sect. 5 comprises the conclusion.

2 Working principle of proposed device

Figure 1 shows the schematic diagram of synchronous up counter using T flip-flops. There are sixteen MZIs that are being used in the implementation of proposed device. MZIs 1, 2, 3, 4 are connected in such a way that they operate as a T flip-flop. The optical signal is constantly being fed in first input port of MZI1. Input electrical signal (T_n) is applied to second electrode of MZI1. Optical signals from first and second output port of MZI1 are fed to first and second input ports of MZI2 respectively, second electrode of which is connected to electrical equivalent of previous complement output of T flip-flop (i.e. electrical equivalent from first output port of MZI3). Similarly, optical signals from first and second output ports of MZI2 appear at first input ports of MZIs 4 and 3 respectively. A clock signal (CLK) is constantly being applied to second electrodes of MZIs 3 and 4. Electrical equivalent of optical signal obtained from first output port of MZI4 (i.e. Q_1) is applied to second electrode of MZI5 (which act as toggle signal for second T flip-flop) and MZI17. In the similar manner, electrical equivalent of optical signal obtained from first output port of MZI8 (i.e. Q_2) is applied to second electrode of MZI18. MZIs 17 and 18 form an AND gate. The electrical equivalent of the AND gate is applied to the second electrodes of MZIs 9 (acting as control signal for third T flip-flop) and 19. Similarly, electrical equivalent of light signal obtained from first output port of MZI12 (i.e. Q_3) is applied to second electrode of MZI20. MZIs 19 and 20 form an AND gate. Again, the electrical equivalent of this AND gate is applied to the second electrode of MZI13. The output Q_4 is obtained from first output port of MZI16. Figure 2 shows the timing CLKs for

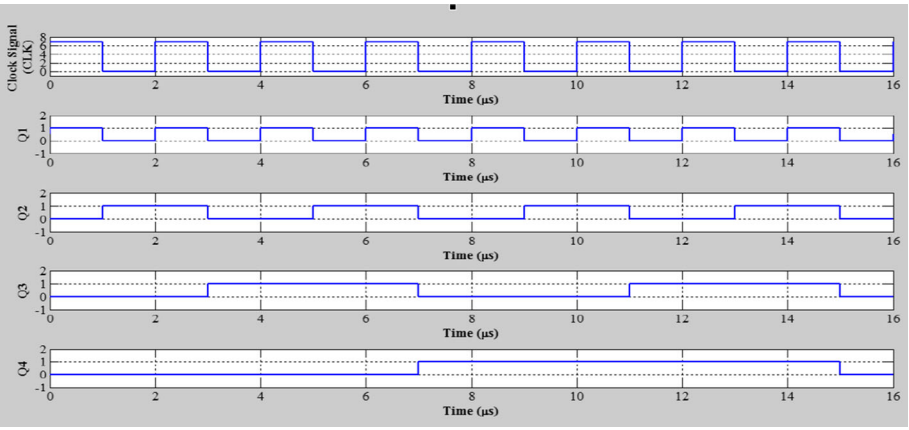

Fig. 2 Sequence of timing signals for 4-bit synchronous up counter

synchronous up counter, in which first row shows the CLK, remaining rows show the output of T flip-flops as Q_1, Q_2, Q_3 and Q_4, respectively.

3 Mathematical expression of device

The mathematical expression for the output of single T flip-flop can be written as follows. The mathematical expression for the output ports of first directional coupler of MZI4 can be written as (Fig. 3)

$$A = \sqrt{1-\alpha_1}(T_0) + j\sqrt{\alpha_1}(Q_{n-1}) \tag{1}$$

$$B = j\sqrt{\alpha_1}(T_0) + \sqrt{1-\alpha_1}(Q_{n-1}) \tag{2}$$

where, T_0 can be written as (Kumar et al. 2014a)

$$T_0 = \sin^2\left(\frac{\Delta\varphi_{MZI_1}}{2}\right)\sin^2\left(\frac{\Delta\varphi_{MZI_2}}{2}\right) + \cos^2\left(\frac{\Delta\varphi_{MZI_1}}{2}\right)\cos^2\left(\frac{\Delta\varphi_{MZI_2}}{2}\right)$$

α_1 is attenuation constant of first directional coupler represented towards the input side of MZI4. In matrix form, Eqs. (1) and (2) can be represented as follows;

$$\begin{bmatrix} A \\ B \end{bmatrix} = \begin{bmatrix} \sqrt{1-\alpha_1} & j\sqrt{\alpha_1} \\ j\sqrt{\alpha_1} & \sqrt{1-\alpha_1} \end{bmatrix} \begin{bmatrix} T_0 \\ Q_{n-1} \end{bmatrix} \tag{3}$$

In the same manner, the expression for the input ports of the second directional coupler of MZI4 be written as,

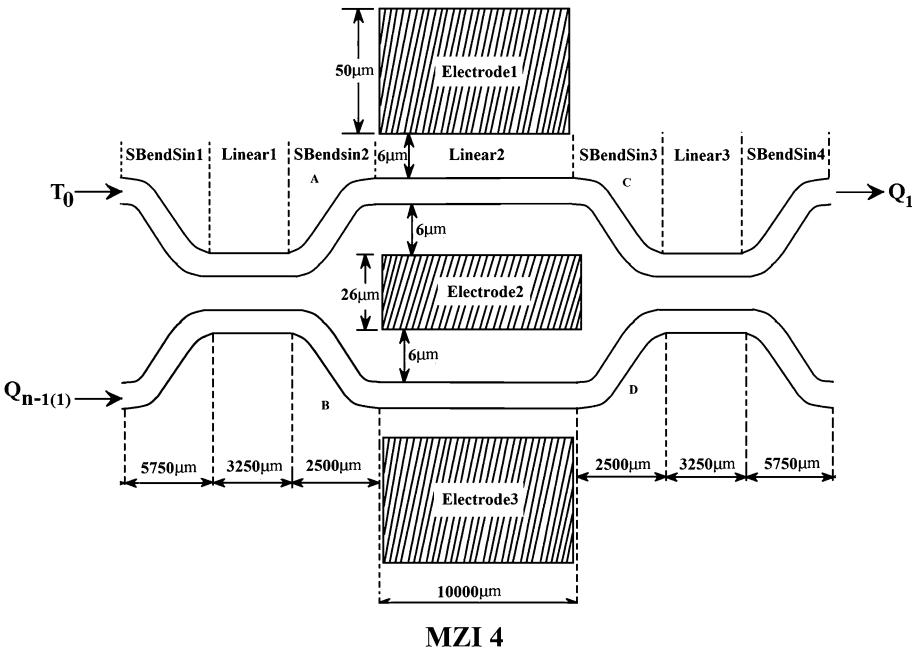

Fig. 3 Schematic diagram of a single MZI

$$C = Ae^{-j\varphi_1}, \quad D = Be^{-j\varphi_2}$$

In matrix form, it can be represented as;

$$\begin{bmatrix} C \\ D \end{bmatrix} = \begin{bmatrix} e^{-j\varphi_1} & 0 \\ 0 & e^{-j\varphi_2} \end{bmatrix} \begin{bmatrix} A \\ B \end{bmatrix} \tag{4}$$

In case of second coupler, the equation can be written to obtain the output signals as follows;

$$OUT_1 = Q_n = \sqrt{1-\alpha_2}(C) + j\sqrt{\alpha_2}(D) \tag{5}$$

$$OUT_2 = j\sqrt{\alpha_2}(C) + \sqrt{1-\alpha_2}(D) \tag{6}$$

In Eqs. (5) and (6), α_2 represents the attenuation constant of the second directional coupler, represented towards the output side of MZI4. Equations (5) and (6) can be represented in matrix form as follow,

$$\begin{bmatrix} OUT_1 \\ OUT_2 \end{bmatrix} = \begin{bmatrix} Q_n \\ OUT_2 \end{bmatrix} = \begin{bmatrix} \sqrt{1-\alpha_2} & j\sqrt{\alpha_2} \\ j\sqrt{\alpha_2} & \sqrt{1-\alpha_2} \end{bmatrix} \begin{bmatrix} C \\ D \end{bmatrix} \tag{7}$$

Now putting the value of C, D, A and B from Eqs. (3) and (4) in Eq. (7) we get;

$$\begin{aligned} \begin{bmatrix} OUT_1 \\ OUT_2 \end{bmatrix} &= \begin{bmatrix} Q_n \\ OUT_2 \end{bmatrix} \\ &= \begin{bmatrix} \sqrt{1-\alpha_2} & j\sqrt{\alpha_2} \\ j\sqrt{\alpha_2} & \sqrt{1-\alpha_2} \end{bmatrix} \begin{bmatrix} e^{-j\varphi_1} & 0 \\ 0 & e^{-j\varphi_2} \end{bmatrix} \begin{bmatrix} \sqrt{1-\alpha_1} & j\sqrt{\alpha_1} \\ j\sqrt{\alpha_1} & \sqrt{1-\alpha_1} \end{bmatrix} \begin{bmatrix} T_0 \\ Q_{n-1} \end{bmatrix} \end{aligned} \tag{8}$$

Simplifying the above equation, the expression for the output of T flip-flop can be written as follow

$$\begin{bmatrix} Q_n \\ OUT_2 \end{bmatrix} = \begin{bmatrix} \sqrt{(1-\alpha_1)(1-\alpha_2)}e^{-j\varphi_1} - \sqrt{\alpha_1\alpha_2}e^{-j\varphi_2} & j\left\{\sqrt{\alpha_1(1-\alpha_2)}e^{-j\varphi_1} + \sqrt{\alpha_2(1-\alpha_1)}e^{-j\varphi_2}\right\} \\ j\left\{\sqrt{\alpha_1(1-\alpha_2)}e^{-j\varphi_1} + \sqrt{\alpha_2(1-\alpha_1)}e^{-j\varphi_2}\right\} & -\sqrt{\alpha_1\alpha_2}e^{-j\varphi_1} + \sqrt{(1-\alpha_1)(1-\alpha_2)}e^{-j\varphi_2} \end{bmatrix} \begin{bmatrix} T_0 \\ Q_{n-1} \end{bmatrix}$$

Hence it can be written as,

$$\begin{aligned} Q_n = \Big[&\left\{\sqrt{(1-\alpha_1)(1-\alpha_2)}e^{-j\varphi_1} - \sqrt{\alpha_1\alpha_2}e^{-j\varphi_2}\right\}T_0 \\ &+ j\left\{\sqrt{\alpha_1(1-\alpha_2)}e^{-j\varphi_1} + \sqrt{\alpha_2(1-\alpha_1)}e^{-j\varphi_2}\right\}Q_{n-1}\Big] \end{aligned} \tag{9}$$

Here, $\varphi_1 = \left(\pi/V_\pi\right)V_1$ and $\varphi_2 = \left(\pi/V_\pi\right)V_2$. V_π is the voltage at which the phase difference between the optical signal across the two arms of interferometers is π. In order to achieve the highest extinction ratio $\alpha_1 = \alpha_2 = 0.5$. The extinction ratio can be represent as the ratio of the maximum and the minimum power levels of the transfer function. Hence, if the minimum power level of the transfer function is zero, then extinction ratio is infinite. To achieve the highest extinction ratio, 50 % of the power-splitting ratio for optical couplers is required. Hence, ideally the couplers used in designing the device must have the attenuation constants 0.5. Hence, we can write,

$$Q_n = \left[\frac{e^{-j\varphi_1} - e^{-j\varphi_2}}{2}\right] T_0 + \left[j\frac{\left\{e^{-j\varphi_1} + e^{-j\varphi_2}\right\}}{2}\right] Q_{n-1}$$

$$Q_n = \left[\frac{e^{-j((\varphi_1+\varphi_2+\varphi_1-\varphi_2)/2)} - e^{-j((\varphi_1+\varphi_2-\varphi_1+\varphi_2)/2)}}{2}\right] T_0 + \left[j\frac{\left\{e^{-j((\varphi_1+\varphi_2+\varphi_1-\varphi_2)/2)} + e^{-j((\varphi_1+\varphi_2-\varphi_1+\varphi_2)/2)}\right\}}{2}\right] Q_{n-1}$$

$$Q_n = e^{-j(\varphi_1+\varphi_2)/2}\left[\frac{e^{-j(\varphi_1-\varphi_2)/2} - e^{j(\varphi_1-\varphi_2)/2}}{2}\right] T_0 + je^{-j(\varphi_1+\varphi_2)/2}\left[\frac{e^{-j(\varphi_1-\varphi_2)/2} + e^{j(\varphi_1-\varphi_2)/2}}{2}\right] Q_{n-1}$$

Assuming that $(\varphi_1 + \varphi_2)/2 = \varphi_0$ and $(\varphi_1 - \varphi_2) = \Delta\varphi$. In the same manner, it can be written as

$$Q_n = e^{-j\varphi_0}\left[\left\{\frac{e^{-j(\Delta\varphi/2)} - e^{j(\Delta\varphi/2)}}{2}\right\} T_0 + j\left\{\frac{e^{-j(\Delta\varphi/2)} + e^{j(\Delta\varphi/2)}}{2}\right\} Q_{n-1}\right]$$

$$Q_n = e^{-j\varphi_0}\left[-j\,sin\left(\frac{\Delta\varphi}{2}\right) T_0 + j\,cos\left(\frac{\Delta\varphi}{2}\right) Q_{n-1}\right]$$

$$|Q_n|^2 = sin^2\left(\frac{\Delta\varphi}{2}\right)|T_0|^2 + cos^2\left(\frac{\Delta\varphi}{2}\right)|Q_{n-1}|^2 + |T_0||Q_{n-1}|sin(\Delta\varphi) \tag{10}$$

Similarly for $\bar{Q}_n$ we can write,

$$T_1 = \cos^2\left(\frac{\Delta\varphi_{MZI_1}}{2}\right)\sin^2\left(\frac{\Delta\varphi_{MZI_2}}{2}\right) + \sin^2\left(\frac{\Delta\varphi_{MZI_1}}{2}\right)\cos^2\left(\frac{\Delta\varphi_{MZI_1}}{2}\right) \tag{11}$$

$$|\bar{Q}_n|^2 = sin^2\left(\frac{\Delta\varphi}{2}\right)|T_1|^2 + cos^2\left(\frac{\Delta\varphi}{2}\right)|\bar{Q}_{n-1}|^2 + |T_1||\bar{Q}_{n-1}|sin(\Delta\varphi) \tag{12}$$

where T_1 is the signal obtained at second output port of MZI2.

In the similar manner, mathematical expressions for remaining three T flip-flops can be obtained.

4 Implementation of 4-bit synchronous up counter using BPM

Beam propagation method (BPM) has been used to analyze the proposed structures. BPM enables us to create the design for a variety of integrated and fiber optics guided wave problems. It works on the principle of finite difference beam propagation method (FD-BPM).

Figure 4 shows BPM layout for 4-bit synchronous up counter and Fig. 5 shows its simulation results. Here, four T flip-flops are connected in cascaded form. The electrical equivalent of light signal obtained from first output port of MZI4 is applied to second electrodes of MZI5 and MZI17. Similarly, electrical equivalents from outputs of MZIs 8 and 12 are applied to second electrodes of MZIs 18 and 20, respectively. A common CLK

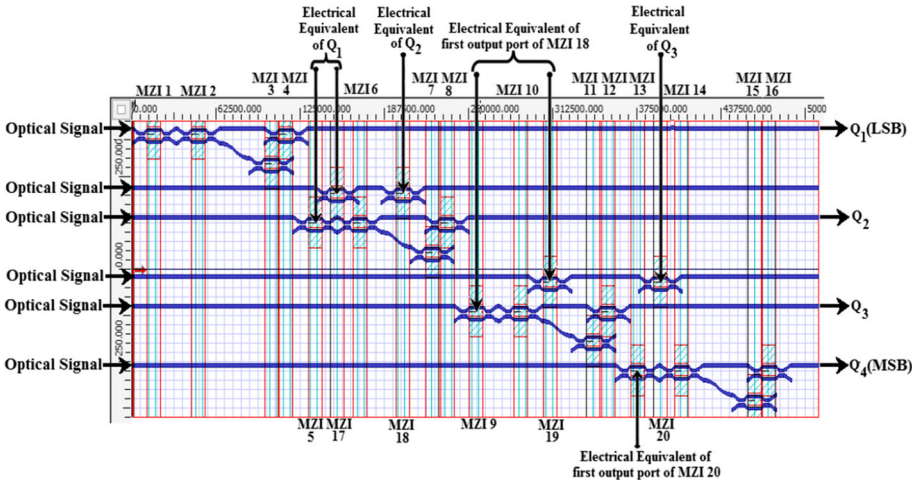

Fig. 4 BPM layout of 4-bit synchronous up counter

is applied to second electrodes of MZIs 3, 4, 7, 8, 11, 12, 15 and 16. Electrical equivalents of light outputs obtained from first output port of MZI18 is applied to second electrodes of MZIs 9 and 19.

The following different cases are possible with the arrival of each clock pulse.

4.1 Case 1: Arrival of first clock pulse

Prior to arrival of first clock pulse, it is assumed that all the flip-flops are reset, ($Q_1 = Q_2 = Q_3 = Q_4 = 0$). Due to which 0 V electrode voltage (electrical equivalents of Q_1, Q_2 and Q_3) is applied to second electrodes of MZIs 5, 17, 18 and 20. It means that T_{n2} (second electrode of MZI5) for second T flip-flop is equal to 0. Since, MZIs 17 and 18 constitutes an AND gate and also 0 V is applied to their second electrodes, no light signal is available at first output port of MZI18. So, 0 V (electrical equivalent of light signal from first output port of MZI18) is applied to second electrodes of MZIs 19 and 9, meaning thereby $T_{n3} = 0$ for third T flip-flop. MZIs 19 and 20 form another AND gate and also since, 0 V is applied to their second electrodes, no light signal comes out of first output port of MZI20. Due to which, 0 V is applied to second electrode of MZI13 (i.e. T_{n4} for fourth flip-flop). At the arrival of first clock pulse, Q_1 toggles to 1 (i.e. light signal is available at first output port of MZI4), because of $T_{n1} = \bar{Q}_{n-1(1)} = Clock\ signal = 1$ for first T flip-flop. Simultaneously, $Q_2 = Q_3 = Q_4 = 0$, because $T_n = 0$ and $T_{n1} = \bar{Q}_{n-1(1)} = Clock\ signal = 1$ for the remaining three T flip-flops. Hence, $Q_1 = 1$, $Q_2 = Q_3 = Q_4 = 0$ as shown in Fig. 5a.

4.2 Case 2: Arrival of second clock pulse

Since, $Q_1 = 1$ in previous case, an electrical equivalent of 6.75 V is applied to second electrodes of MZIs 5 (i.e. T_{n2}) and 17. Similarly, 0 V is applied to second electrode of MZI18, due to $Q_2 = 0$ in previous case. MZIs 17 and 18 form an AND gate, electrical equivalent of which is 0 V (because of 6.75 and 0 V applied to second electrodes of MZIs

17 and 18 respectively). This 0 V is applied to second electrodes of MZIs 9 (i.e. T_{n3}) and 19. In the similar manner, 0 V is applied to second electrode of MZI20 (because $Q_3 = 0$ in previous case). MZIs 19 and 20 form an AND gate, electrical output of which is 0 V

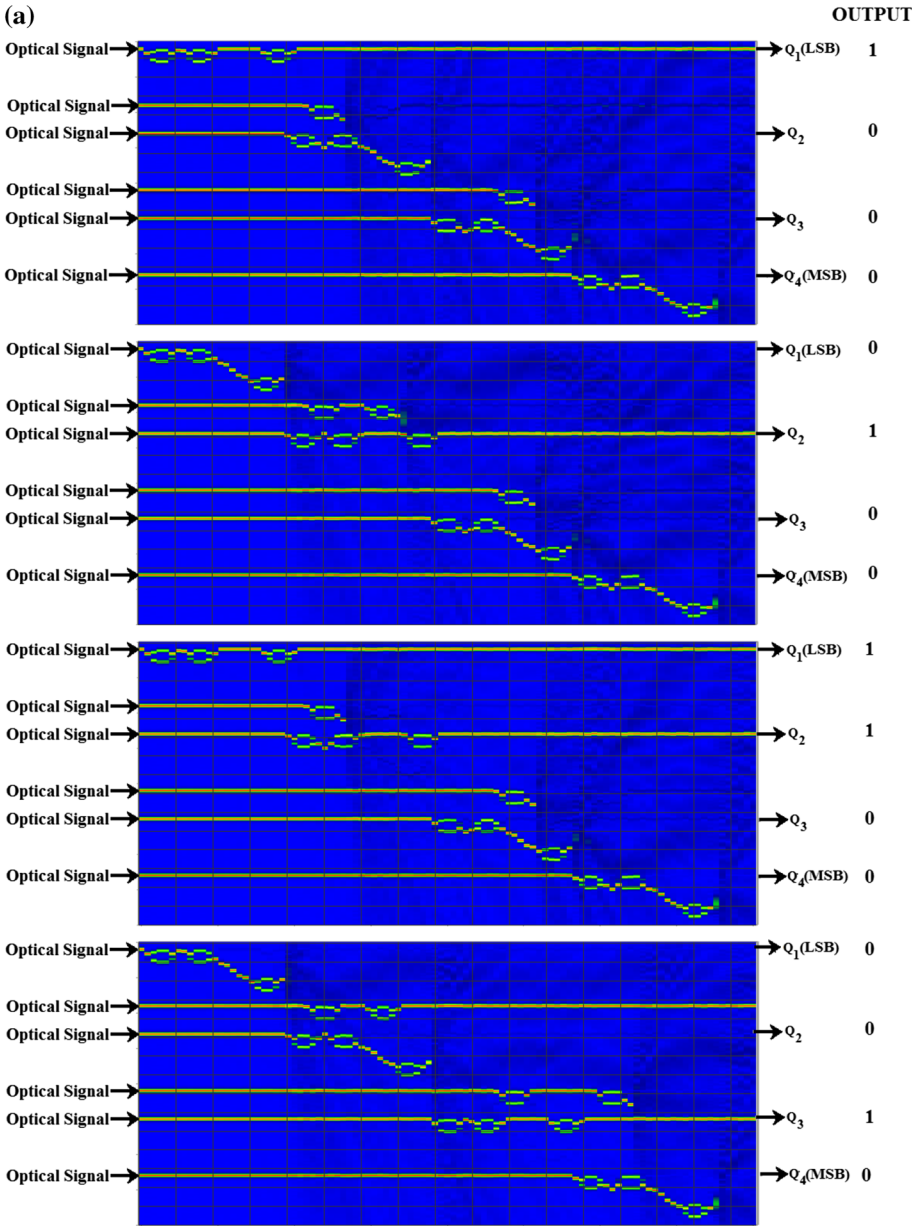

Fig. 5 **a** Simulation result of proposed 4-bit synchronous up counter using BPM for different outputs (1000–0010). **b** Simulation result of proposed 4-bit synchronous up counter using BPM for different outputs (1010–0001). **c** Simulation result of proposed 4-bit synchronous up counter using BPM for different outputs (1001–0011). **d** Simulation result of proposed 4-bit synchronous up counter using BPM for different outputs (1011–0000)

(because 0 V is applied to electrodes of MZIs 19 and 20). This 0 V is applied to second electrode of MZI13 (T_{n4}). Simultaneously, 0 V is available at second electrodes of MZI2, because $\bar{Q}_1 = 0$ in case 1. Similarly, 6.75 V is available at second electrodes of MZIs 6, 10 and 14, because $\bar{Q}_2 = \bar{Q}_3 = \bar{Q}_4 = 1$. At the arrival of second clock pulse, Q_1 toggles to 0 (i.e. no light signal is available at first output port of MZI4), because of $T_{n1} = \bar{Q}_{n-1(1)} = 0$,

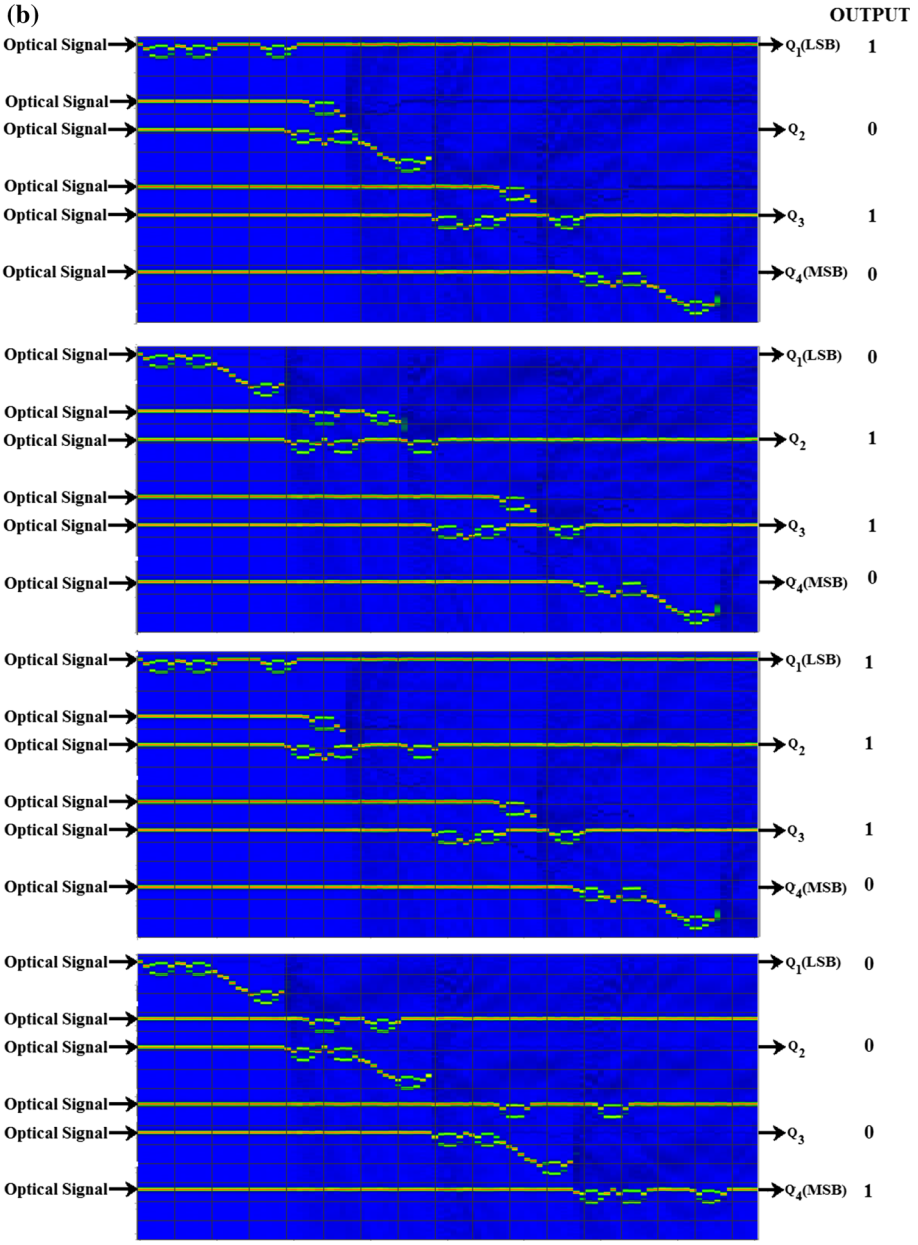

Fig. 5 continued

Clock signal = 1. Simultaneously, $Q_2 = 1$ (because, $T_{n1} = \bar{Q}_{n-1(2)} = 1$, *Clock signal* = 1 for second flip-flop), $Q_3 = Q_4 = 0$, because $T_n = 0$ and $\bar{Q}_{n-1} = Clock\ signal = 1$ for the remaining two T flip-flops. Hence, $Q_2 = 1$, $Q_1 = Q_3 = Q_4 = 0$ as shown in Fig. 5a.

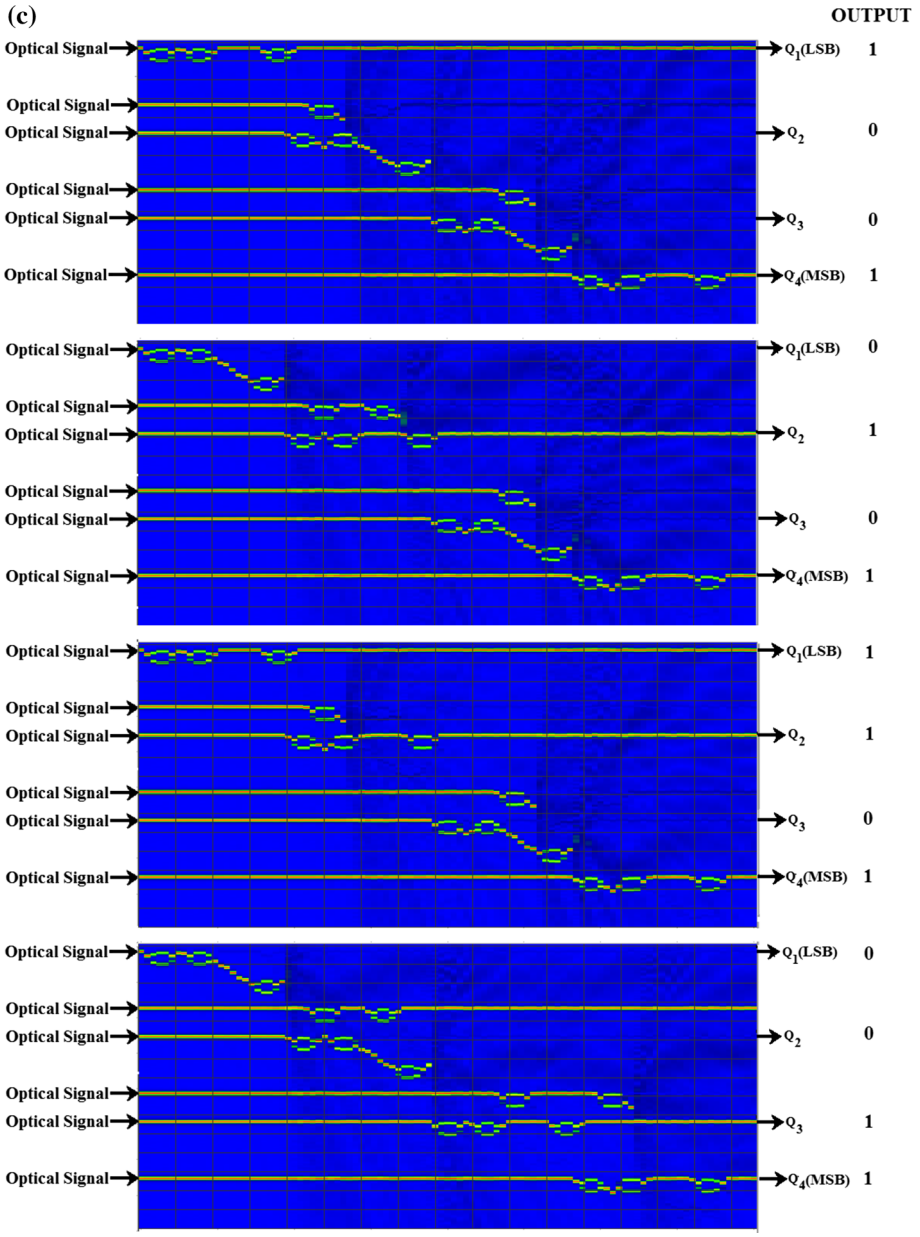

Fig. 5 continued

4.3 Case 3: Arrival of third clock pulse

In this case, $\bar{Q}_{n-1(1)} = 1$, $\bar{Q}_{n-1(2)} = 0$, $\bar{Q}_{n-1(3)} = 1$ and $\bar{Q}_{n-1(4)} = 1$ as seen from second case. Also, $T_{n1} = 1$, $T_{n2} = 0$, $T_{n3} = 0$, $T_{n4} = 0$. At the arrival of clock pulse, light outputs at output of T flip-flops become $Q_1 = Q_2 = 1$, $Q_3 = Q_4 = 0$ as shown in Fig. 5a.

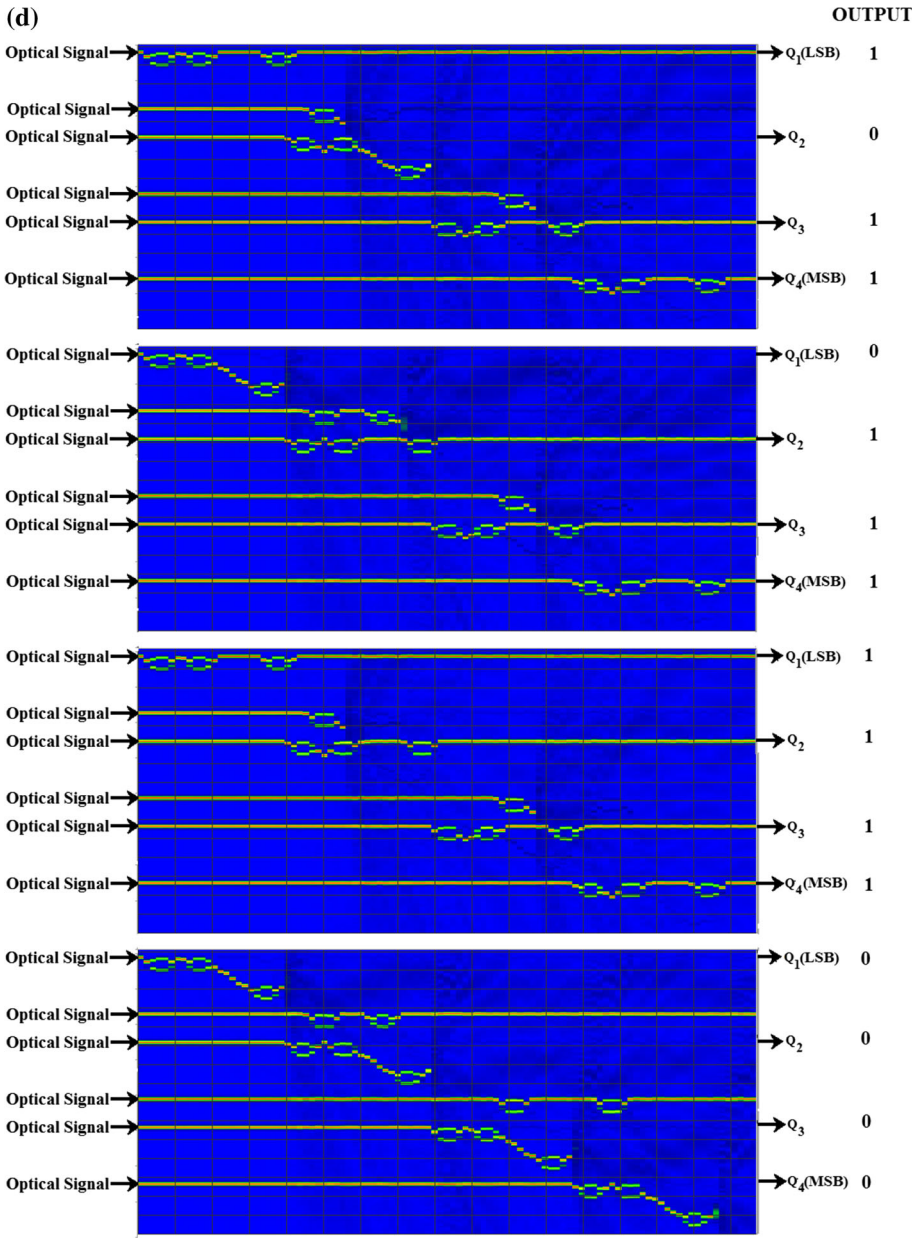

Fig. 5 continued

Table 1 Function table for 4-bit synchronous up counter

S. No.	CLK	T_{n1} (V)	T_{n2} (V)	T_{n3} (V)	T_{n4} (V)	Q_4	Q_3	Q_2	Q_1
1.	↑	6.75	0	0	0	0	0	0	1
2.	↑	6.75	6.75	0	0	0	0	1	0
3.	↑	6.75	0	0	0	0	0	1	1
4.	↑	6.75	6.75	6.75	0	0	1	0	0
5.	↑	6.75	0	0	0	0	1	0	1
6.	↑	6.75	6.75	0	0	0	1	1	0
7.	↑	6.75	0	0	0	0	1	1	1
8.	↑	6.75	6.75	6.75	6.75	1	0	0	0
9.	↑	6.75	0	0	0	1	0	0	1
10.	↑	6.75	6.75	0	0	1	0	1	0
11.	↑	6.75	0	0	0	1	0	1	1
12.	↑	6.75	6.75	6.75	0	1	1	0	0
13.	↑	6.75	0	0	0	1	1	0	1
14.	↑	6.75	6.75	0	0	1	1	1	0
15.	↑	6.75	0	0	0	1	1	1	1
16.	↑	6.75	6.75	6.75	6.75	0	0	0	0

4.4 Case 4: Arrival of fourth clock pulse

In this case, $\bar{Q}_{n-1(1)} = 0$, $\bar{Q}_{n-1(2)} = 0$, $\bar{Q}_{n-1(3)} = 1$ and $\bar{Q}_{n-1(4)} = 1$ as seen from third case. Also, $T_{n1} = 1$, $T_{n2} = 1$, $T_{n3} = 1$, $T_{n4} = 0$. At the arrival of clock pulse, light outputs at output of T flip-flops become $Q_1 = Q_2 = 0$, $Q_3 = 1$, $Q_4 = 0$ as shown in Fig. 5a.

4.5 Case 5: Arrival of fifth clock pulse

In this case, $\bar{Q}_{n-1(1)} = 1$, $\bar{Q}_{n-1(2)} = 1$, $\bar{Q}_{n-1(3)} = 0$ and $\bar{Q}_{n-1(4)} = 1$ as seen from fourth case. Also, $T_{n1} = 1$, $T_{n2} = 0$, $T_{n3} = 0$, $T_{n4} = 0$. At the arrival of clock pulse, light outputs at output of T flip-flops become $Q_1 = 1$, $Q_2 = 0$, $Q_3 = 1$, $Q_4 = 0$ as shown in Fig. 5b.

In the similar fashion, up counting up to $Q_1 = Q_2 = Q_3 = Q_4 = 1$ takes place on the arrival of positive clock pulses as shown in Fig. 5b–d. After that, counter resets i.e. $Q_1 = Q_2 = Q_3 = Q_4 = 0$.

The function table for 4-bit synchronous up counter is shown in Table 1. Where, Q_4 is considered as MSB and Q_1 as LSB. It can be clearly seen that the table is getting verified from results obtained from BPM, which is discussed earlier.

5 Conclusion

An optical 4-bit synchronous up counter based on the EO effect of MZI has been demonstrated. The layout diagram of the proposed device is presented along with the appropriate mathematical description and the results are verified using BPM. The results furnished in this paper will be a stepping stone in the area of designing WDM optical components and optical signal processing units.

Acknowledgments This work is supported by the project entitled "Performance study of some WDM optical network components and design of optical switching devices" under the Faculty Research Scheme of DIT University, Dehradun India (Ref. No.: DITU/R&D/2014/7/ECE) undertaken by Dr. Santosh Kumar. The authors would also like to thank Prof. K. K. Raina, Vice Chancellor, DIT University, India for encouragement and support during the present research work.

References

Caulfield, H.J.: The unique advantages of optics over electronics for interconnections. Proc. SPIE **1390**, 399–402 (1990)

Caulfield, H.J., Collins Jr, S.A.: Optical holographic interconnects: categorization and potential efficient passive resonated holograms. J. Opt. Soc. Am. **6**, 1568–1577 (1989)

Caulfield, H.J., Shamir, J.: Wave particle duality considerations in optical computing. Appl. Opt. **28**, 2184–2186 (1989)

Caulfield, H.J., Shamir, J.: Wave-particle-duality processors: characteristics, requirements and applications. J. Opt. Soc. Am. **7**, 1314–1323 (1990)

Feuerstein, R.J., Soukup, T., Heuring, V.P.: 100-MHz optical counter that uses directional coupler switches. Opt. Lett. **16**(20), 1599–1601 (1991)

Goodman, J.W., Leonberger, F.I., Kung, S.Y., Athale, R.A.: Optical interconnections for VLSI systems. Proc. IEEE **72**, 850–866 (1984)

Jin, H., Liu, F.M., Xu, P., Xia, J.L., Zhong, M.L., Yuan, Y., Zhou, J.W., Gong, Y.X., Wang, W., Zhu, S.N.: On-chip generation and manipulation of entangled photons based on reconfigurable lithium-niobate waveguide circuits. Phys. Rev. Lett. **113**, 103601–103605 (2014)

Kaur, S., Kaler, R.S.: 5 GHz all-optical binary counter employing SOA-MZIs and an optical NOT gate. J. Opt. **16**(3), 5201 (2014)

Kumar, S., Raghuwanshi, S.K., Kumar, A.: Implementation of optical switches by using Mach–Zehnder interferometer. Opt. Eng. **52**(9), 097106 (2013)

Kumar, A., Kumar, S., Raghuwanshi, S.K.: Implementation of full-adder and full-subtractor based on electro-optic effect in Mach–Zehnder interferometer. Opt. Commun. **324**, 93–107 (2014a)

Kumar, A., Kumar, S., Raghuwanshi, S.K.: Implementation of XOR/XNOR and AND logic gates using Mach–Zehnder interferometers. Optik **125**, 5764–5767 (2014b)

Kumar, S., Bisht, A., Singh, G., Choudhary, K., Sharma, D.: Implementation of wavelength selector based on electro-optic effect in Mach–Zehnder interferometers for high speed communications. Opt. Commun. **350**, 108–118 (2015a)

Kumar, S., Singh, G., Bisht, A.: 4×4 signal router based on electro-optic effect of Mach–Zehnder interferometer for wavelength division multiplexing applications. Opt. Commun. **353**, 17–26 (2015b)

Li, G., Qian, F., Ruan, H., Liu, L.: Compact parallel optical modified-signed-digit arithmetic-logic array processor with electron-trapping device. Appl. Opt. **38**(23), 5039–5045 (1999)

Poustie, A., Manning, R.J., Kelly, A.E., Blow, K.J.: All-optical binary counter. Opt. Express **6**(3), 69–74 (2000)

Raghuwanshi, S.K., Kumar, A., Kumar, S.: 1×4 signal router using three Mach–Zhender interferometers. Opt. Eng. **52**(03), 035002 (2013)

Raghuwanshi, S.K., Kumar, A., Chen, N.K.: Implementation of sequential logic circuits using the Mach–Zehnder interferometer structure based on electro-optic effect. Opt. Commun. **333**, 193–208 (2014)

Shen, Z.Y., Wu, L.L.: Reconfigurable optical logic unit with a terahertz optical asymmetric demultiplexer and electro-optic switches. Appl. Opt. **47**(21), 3737–3742 (2008)

Singh, G., Janyani, V., Yadav, R.P.: Modeling of a high performance Mach–Zehnder interferometer all optical switch. Opt. Appl. **42**, 613–625 (2012)

Sokoloff, J.P., Prucnal, P.R., Glesk, I., Kane, M.: A terahertz optical asymmetric demultiplexer (TOAD). IEEE Photonics Technol. Lett. **5**(7), 787–789 (1993)

Vikram, C.S., Caulfield, H.J.: Position-sensing detector for logical operations using incoherent light. Opt. Eng. **44**, 115201–115204 (2005)

Wang, B.C., Baby, V., Tong, W., Xu, L., Friedman, M., Runser, R.J., Glesk, I., Prucnal, P.R.: A novel fast optical switch based on two cascaded terahertz asymmetric demultiplexers (TOAD). Opt. Express **10**(1), 15–23 (2002)

Wang, J., Meloni, G., Berrettini, G., Potì, L., Bogoni, A.: All-optical binary counter based on semiconductor optical amplifiers. Opt. Lett. **34**(22), 3517–3519 (2009)

Wooten, EdL, Kissa, K.M., Yan, A.Y., Murphy, E.J., Lafaw, D.A., Hallemeier, P.F., Maack, D., Attanasio, D.V., Fritz, D.J., McBrien, G.J., Bossi, D.E.: A review of lithium niobate modulators for fiber-optic communications systems. IEEE J. Sel. Top. Quantum Electron. **6**(1), 69–82 (2000)